Design of Polyuretanes and Related Hydrogen-Bonding Supramolecular Materials with Charge Carrier Transporting Properties

Tsuneaki Sakurai,[1] Shu Seki,*[1] Suhrit Ghosh,[2] Kazunori Sugiyasu[3], Masayuki Takeuchi,[3]

[1] *Department of Molecular Engineering, Graduate School of Engineering, Kyoto University.*
Nishikyo-ku, Kyoto 615-8510, Japan
[2] *Polymer Science Unit, Indian Association for the Cultivation of Science, Kolkata-700032, India*
[3] *Molecular Design & Function Group, National Institute for Materials Science (NIMS), 1-2-1 Sengen, Tsukuba, Ibaraki 305-0047, Japan*

（第一回　ポリウレタン国際技術振興財団研究助成）

Introduction

Polyurethane is a widely used polymer backbone carrying multiple urethane bonds. These urethane linkages are capable of forming both intramolecular and intermolecular hydrogen (H-) bonds in both solution and solid state, affording various kinds of supramolecular materials with organized structures.[1–3] Controlled H-bondings can be realized by periodically arranging urethane bonds as well as analogous amide and urea functionalities in polymer main chains. One of the unique conformationally organized structures for those polymers is folded state as a single polymer chain. Such folding polymers have been categorized into “foldamer”, where helical or layered nanostructures are formed with the help of periodic H-bonding formations among adjacent/nonadjacent monomer units.[4–6] Classical polyurethane itself has elastic or thermoplastic characters, but no optical or conductive properties are equipped due to the absence of conjugated moieties. However, by means of the polyurethane scaffold providing periodically aligned urethane functionalities, it is possible to incorporate π-conjugated units into either main or side chains periodically.

In our study, naphthalenediimide (NDI), a famous n-type semiconducting π-conjugated motif, was introduced as a pendant group of a classical polyurethane backbone. The charge carrier transporting property was studied by our noncontact microwave-based technique.[7,8] As a result, significantly larger electron mobility and longer lifetime of charge carriers were observed for the folded tubular assembly of the NDI-appended polyurethane than those for unfolded polymer, likely due to a better delocalization of the charge carriers in the integrated tubular assembly consisting of stacked NDI arrays inside the multilayer wall.[9]

Furthermore, inspired by this polyurethane scaffold having H-bonding units, we

developed porphyrin-based supramolecular polymers with three types of nanostructures. Nanofiber, nanosheet, and nanoparticle morphologies were developed from the identical monomer by finely tuning the π-π stacking, H-bonding, and van der Waals interactions among alkyl chains that can be controlled by the preparation conditions. The observed photoconductivity and charge carrier mobility for these nanostructured films were found to be different, reflecting the nanostructures providing different charge transporting pathways.[10]

Principle of noncontact assessment technique of charge carrier mobility in soft-molecular aggregates.

Till date, highly sophisticated assessment techniques have been developed for the analysis of charge carrier mobility such as time-of-flight (TOF),[11] field-effect-transistor (FET),[12] space-charge-limited-current (SCLC),[13] impedance spectroscopy (IS) analyses.[14] The analyses give the value of mobility as a consequence of long-range translational motion of charge carriers along electric field vector E applied between a set of electrodes apart as a few hundreds mm. The statistically deduced value of mobility is often impacted by the presence of charge carrier injection barriers at the electrode interfaces, structural instability and defects, impurities, etc, leading to screen the intrinsic potentials of the charge conducting nature of the materials. Particularly in case of molecular assembly, even if the structure has been stabilized via relatively strong hydrogen bonding networks, the fabrication procedures of the devices for the mobility assessments cause severe damages on the structures/interfaces, resulting in the far lower values of mobility than the ones originally the materials are expected. This is the case of the strong demands for the contactless evaluation of charge carrier mobility in soft molecular materials, and we have developed a series of assessment techniques refers as time-resolved microwave conductivity (TRMC) measurements via the short-range interaction of electromagnetic waves in GHz range (microwaves) and charge carriers photo-injected into the molecular assembly without electrodes attached.[7,8,15–17]

Short-range (nm-scaled) oscillating motion is induced by the interaction between microwaves and charge carriers, and the fundamental Maxwell's formulae on the interaction are given as followings in semiconducting materials with negligible conductivity of σ.

$$\Delta E = \frac{\partial}{\partial t}\left(\mu_{\mathrm{m}} \varepsilon_{\mathrm{m}} \frac{\partial}{\partial t} E + \mu_{\mathrm{m}} \sigma E \right) \qquad (1),$$

$$\Delta B = \frac{\partial}{\partial t}\left(\mu_{\mathrm{m}} \varepsilon_{\mathrm{m}} \frac{\partial}{\partial t} B + \mu_{\mathrm{m}} \sigma B \right) \qquad (2),$$

where B is magnetic field, μ_m and ε_m are magnetic permeability and permittivity, respectively. In case of $E(r)$ (and $B(r)$) given as a sinusoidal standing wave, the

simultaneous equations of (1) and (2) are converted in terms of E(t) as,

$$\Delta E(r) = \mu_{\mathrm{m}} \left(i\sigma\omega - \varepsilon_{\mathrm{m}}\omega^2 \right) E(r) \quad (3)$$

Thus, the complex dielectric constant of the medium with small electrical conductivity is given as,

$$\varepsilon = \varepsilon_m - i\frac{\sigma}{\omega}, \quad (4),$$

and the above Maxwell equation is rearranged and simplified using ε as

$$\Delta E(r) = \varepsilon\mu_m\omega^2 E(r) \quad (5).$$

This is suggestive of a direct correlation with the complex dielectric constant and conductivity of the materials. As seen in eqs. (4) and (5), the trace of $E(t)$ gives directly complex ε, and deducing quantitatively and separately the contribution of imaginary part in ε immediately allow us to estimate σ of the materials in the interaction.

The value of mobility (μ), the final target of the assessment, is in direct relation with conductivity as,

$$\sigma = en\mu \quad (6),$$

where e and n are elementary charge and charge carrier density, respectively. Mobility measurement along with the above scheme is advantageous to realize a non-contact, non-destructive screening process without the need for device fabrication. However unlike the conventional measurement techniques, electrical amplification techniques are not applicable for this scheme via evolution of current (voltage) by external amplifier systems. To achieve highly sensitivity in the measurement with wide dynamic range, a microwave cavity system is the primary choice to promote effective interactions of probing microwave with the injected charge carriers, facilitating dramatic increase in the sensitivity which is in trade-off relation with response time of the system.[18,19]

Assuming an electromagnetic wave cavity with a Q value, the loss of electromagnetic waves in the cavity ($\Delta 1/Q$) cannot be measured directly by inserting probes, and the power (P_{r}) of microwaves reflected from the cavity and its transient changes (ΔP_{r}) is the only observable. The Q value can be further divided into Q_{u}, Q_{s}, and Q_{c} corresponding to the cavity coupling with waveguide, the interaction with sample in static states, and the interaction with conductive species injected transiently, respectively. The Q_{u} and Q_{s} components remain constant during measurement of microwave power loss, so these can be included in Q. The relationship between Q, Q_{u}, and Q can be expressed as:

$$\frac{1}{Q} = \frac{1}{Q_{\mathrm{S}}} + \frac{1}{Q_{\mathrm{U}}} \quad (7).$$

Prior to carrier injection, the cavity is in resonance at the frequency of f_0 (= $\omega_0/2\pi$). If the

insertion of samples into the cavity only causes perturbation of the cavity parameters, the static loss of microwave is small enough, the change is given as,

$$\frac{1}{Q_S}-\frac{1}{Q_U}\approx\frac{1}{Q_C}-\frac{1}{Q_U}\approx d\left(\frac{1}{Q}\right) \qquad (8).$$

Simultaneously, we define the static shift of microwave resonance angular frequency as $\Delta\omega$. The normalized reflection (P_R) of the microwave from the cavity is now given as,

$$P_R=\frac{4\left(\frac{\Delta\omega}{\omega_0}\right)^2+\left\{d\left(\frac{1}{Q}\right)\right\}^2}{4\left(\frac{\Delta\omega}{\omega_0}\right)^2+\left(\frac{1}{Q}\right)^2} \qquad (9).$$

Herein excess charge carriers are injected non-contactly into the sample via mainly photo-carrier generation processes upon excitation to laser pulses within response time of the measurement system, leading to the change of Q value into Q_c. The P_R after the interaction of the charge carriers changes into P_R' as,

$$P_R'=\frac{4\left(\frac{\Delta\omega}{\omega_0}\right)^2+\left(\frac{1}{Q_C}-\frac{1}{Q_U}\right)^2}{4\left(\frac{\Delta\omega}{\omega_0}\right)^2+\left(\frac{1}{Q}\right)^2} \qquad (10).$$

The net contribution from the dielectric loss by the charge carriers is,

$$\Delta\left(\frac{1}{Q}\right)=\frac{1}{Q_C}-\frac{1}{Q_S} \qquad (11),$$

and the change in the normalized reflected microwave power $\Delta P_R = P_R' - P_R$ reveals to depend linearly on $\Delta 1/Q$ as the following form derived by the rearrangements of eqs (9), (10), and (11),

$$\begin{aligned}\Delta P_R = P_R'-P_R &= \frac{\frac{1}{Q_C}-\frac{1}{Q_S}}{4\left(\frac{\Delta\omega}{\omega_0}\right)^2+\left(\frac{1}{Q}\right)^2}\left\{\frac{1}{Q_S}+\frac{1}{Q_C}-\frac{2}{Q_U}\right\} \\ &= \frac{d\left(\frac{1}{Q}\right)}{2\left(\frac{\Delta\omega}{\omega_0}\right)^2+\frac{1}{2}\left(\frac{1}{Q}\right)^2}\Delta\left(\frac{1}{Q}\right)\end{aligned} \qquad (12).$$

and simplified as,

$$\Delta P_R \propto \Delta\left(\frac{1}{Q}\right) \qquad (13).$$

Now, once back to the eq. (4), the ratio of real and imaginary parts of the dielectric constant is often called as a dielectric loss factor of tanδ as,

$$\tan\delta = \frac{\varepsilon''}{\varepsilon'} = \frac{\sigma}{\omega\varepsilon'} \quad (14).$$

In contrast, the Q factor of the microwave cavity is defined also by the ratio of microwave power storage in the cavity (W) and its consumption (L) as,

$$\frac{1}{Q} = \frac{L}{\omega_0 W} \quad (15).$$

W is estimated simply by the averaged electric field strength of sinusoidal standing waves with angular frequency of $\omega = 2\pi/T$ in the cavity over the time as,

$$W = \varepsilon' < E^2 > = \frac{\varepsilon'}{T}\int {E_0}^2 \cos^2(\omega t)\mathrm{d}t = \frac{\varepsilon' {E_0}^2}{2} \quad (16).$$

For L, we assume Joule's heating by the local oscillating motion of charge carriers via the interaction with microwave. Aaveraged Joule's heating is given by eq. (14) as,

$$L = \sigma E^2 = \omega\varepsilon'' E^2 = \omega\varepsilon' E^2 \tan\delta \quad (17),$$

and averaged over the time as,

$$L = \frac{\omega\varepsilon'\tan\delta}{T}\int {E_0}^2 \cos^2(\omega t)dt = \frac{\omega\varepsilon'\tan\delta {E_0}^2}{2} \quad (18).$$

Substitution of eq. (15) by eqs. (16) and (18) leads,

$$\frac{1}{Q} = \frac{L}{\omega_0 W} = \frac{\omega\varepsilon'\tan\delta {E_0}^2/2}{\omega_0\varepsilon' {E_0}^2/2} = \frac{\omega}{\omega_0}\tan\delta \quad (19),$$

and if the change of micorwave frequency can be neglegible even after the interaction with the transiently injected charge carriers, we obtain,

$$\Delta\frac{1}{Q} = \Delta\tan\delta = \frac{\Delta\sigma}{\omega\varepsilon'} \propto \Delta P_{\mathrm{R}} \quad (20),$$

which is suggestive that the precise tracing of the change in the reflected microwave power from the cavity give immediately an estimates of conductivity change in the materials loaded in the cavity via transietn charge carrier injection.

Combination of transient absorption spectroscopy (TAS) and TRMC for totally non-contact assessment of charge carrier mobility

To deduce finaly the value of mobility of charge carriers, as seen in eq. (6), the number of charge carriers (n) is indispensable for fully experimental assesment. A pioneering work was reported by Warman *et al.* at Delft University of Technology (Netherlands) using microwaves ranging at 10–50 GHz (microwaves) for conductivity measurements combined with transient absorption spectroscopy.[20,21] This technique is referred to as pulse-radiolysis time-resolved microwave conductivity (PR-TRMC), as it

generates transient charge carriers in the materials upon exposure to a pulsed high-energy electron beam. Because of the homogenous ionization of the primary component of the medium, the density of the generated charge carriers can be determined without performing other independent measurements, allowing a direct evaluation of charge carrier mobility from the accurate detection of dielectric loss. In contrast, the authors have focused on the flash-photolysis TRMC (FP-TRMC) utilizing exciton dissociation into charges as a charge-carrier injection scheme.[7,8,15–17] Transient absorption spectroscopy has been combined with the TRMC apparatus, allowing us to simultaneous determination of charge carrier density (n) injected into the materials non-contactly. The details of the total set of apparatus are described in elsewhere.[16,17] The present FP-TRMC systems are successfully applied to reveal the electronic conductive nature of molecular aggregates stabilized by hydrogen bonding networks via urethane moieties, and we discuss in the following sections. In eq. (20), the normalization of ΔP_R is typically carried out by the ratio of actual power reflection from the cavity prior to carrier injection (P_r / W) and its change by the injection (ΔP_r / W) as follows,

$$\Delta P_R = \frac{\Delta P_r}{P_r} \tag{21},$$

and with the proportional factor A in eq. (20):

$$A = \mp \frac{\omega_0 \varepsilon_0 \varepsilon_r}{2Q} \left(\left(\frac{P_i}{P_r} \right)^{\frac{1}{2}} \pm 1 \right)^{-1} \tag{22},$$

we obtain the following equation by the rearrangement of eq. (20) as,

$$\Delta\sigma = A \left(\frac{\Delta P_r}{P_r} \right) \tag{23},$$

where ω and ε' are assumed to be constant as $\omega = \omega_0$ and $\varepsilon' = \varepsilon_0\varepsilon_r$ because of negligibly small amount of injected charge carriers into the system. P_i is the power of microwave injected into the cavity, and typically fixed at 1-10 mW in our system. Transient charge carriers are injected by photo-ionization by ns laser pulses with the duration of a few ns which is short enough to the response time of the cavity system. Here upon photoexcitation, the carrier density of Δn (m^{-3}) is injected into the system, giving the change of electrical conductivity as,

$$\Delta\sigma = e\Delta n \sum \mu \tag{24},$$

where $\Sigma\mu$ ($m^2\ V^{-1}\ s^{-1}$) is the sum of the mobility of negative and positive charge carriers. Unfortunately quantitative contribution from negative (electron) and positive (hole) carriers cannot be discusses separately in case of photo-carrier injection without selective

quenching of carriers by additives. TAS measurement of photo-generated carriers (electrons/radical anions and holes/radical cations) gives simultaneously the kinetic traces $OD(t)$ as well as the quantum efficiency (ϕ) of the transient species with their molar extinction coefficients, and similarity of the kinetic traces of $\Delta\sigma(t)$ and $OD(t)$ can recognize the major contribution from charge carrier species. Under a light excitation with the photon density I_0 (m^{-2}), the number density of absorbed photons can be derived from a linear absorption coefficient of the target molecules F (m^{-1}) as FI_0, and consequently the value of Δn is given by,

$$\Delta n = \phi I_0 F \qquad (25).$$

From eqs. (23) (24) and (25), finally we obtain,

$$\phi \sum \mu = \frac{A}{eI_0 F}\left(\frac{\Delta P_r}{P_r}\right) \qquad (26).$$

With the value of ϕ determined by TAS, TRMC measurement allows us to fully experimental assessment of charge carrier mobility in a variety of materials.[7,8] The present system has been successfully applied to the urethane-based molecular aggregates, leading to the intrinsic charge transport properties.

Synthesis of polyurethane carrying NDI pendants as side chains.

P1 was synthesized (**Scheme 1**) by a step- growth polymerization between hexamethylene-diisocyanate (**M1**) and a NDI-containing diol (**M2**) in the presence of small amount of (s)-(−)-2-methyl 1-butanol as a "mono-functional impurity" with a specific ratio to ensure capping of all the chain-ends by the chiral alcohol. The poly condensation was carried out in the presence of 1,4-diazabicyclo[2.2.2]octane (DABCO) catalyst in THF to produce the desired polyurethane (**P1**) as a light yellow powder in 75% yield. The end g roup analysis in ^{1}H NMR estimated the molecular weight of **P1** to be 8000 Da that matched reasonably well with the number average degree of polymerization =13, estimated from the Carothers's equation. GPC chromatogram of **P1** in THF showed a unimodal distribution with weight-average molecular weight (M_w) = 7600 Da (PDI = 1.72) that corroborated well with the value obtained from end group analysis.

Self-assembled structures of polyurethane carrying NDI pendants.

Self-assembly of **P1** was tested in a nonpolar solvent, methylcyclohexane (MCH). At 5.0 mM concentration, the polymer was soluble at high temperature and upon allowing to settle at room temperature, the solution gradually became more viscous and eventually resulted in a nearly transparent green emitting gel (**Figure 1**) after 72 h at 3.0 mM. To have a closer look at the morphology of the gel, high resolution transmission electron microscopy (HR-TEM)-images were recorded that showed nanotubular structures for the aged sample (**Figure 1**). The inner diameter and wall thickness of the tubes were measured to be 85 ± 5 nm and 26 ± 2 nm, respectively, while the length extended over 5−9 μm. In contrast, the HR-TEM images of a freshly prepared solution showed hollow spherical objects. UV-vis absorption spectra of **P1** in a good solvent such as $CHCl_3$

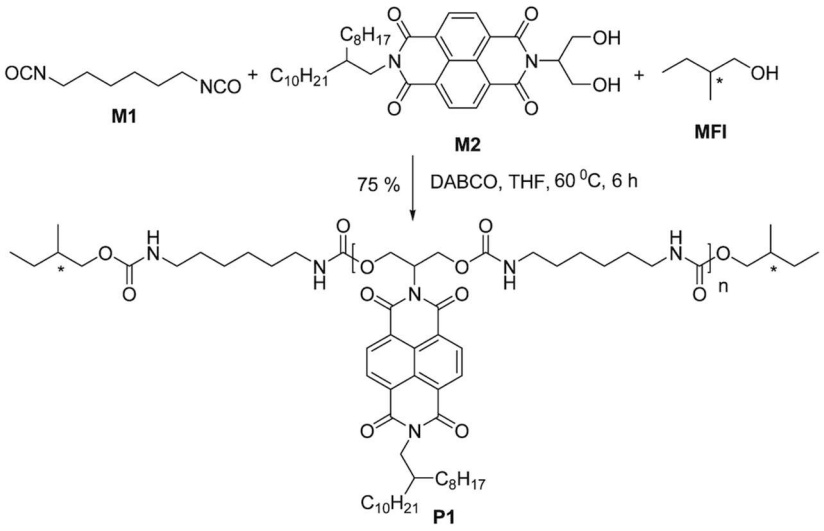

Scheme 1. Synthesis of polyurethane **P1** carrying NDIs.

showed sharp absorption bands in the range of 300–400 nm with obvious vibronic features indicating presence of monomeric NDI -chromophores. Nevertheless, in a nonpolar medium like MCH, a significant lowering of intensity with concomitant reversal of the intensities of the peaks at 382 and 361 nm were noticed owing to π–π interaction. The absorption bands in MCH did not exhibit red-shift as typically observed for offset π-stacking of NDI chromophores, suggesting interchromophoric interaction without longitudinal displacement between the adjacent NDI units. Concentration dependent UV-vis experiments showed no spectral change in the range of 10^{-3}–10^{-5} M with the

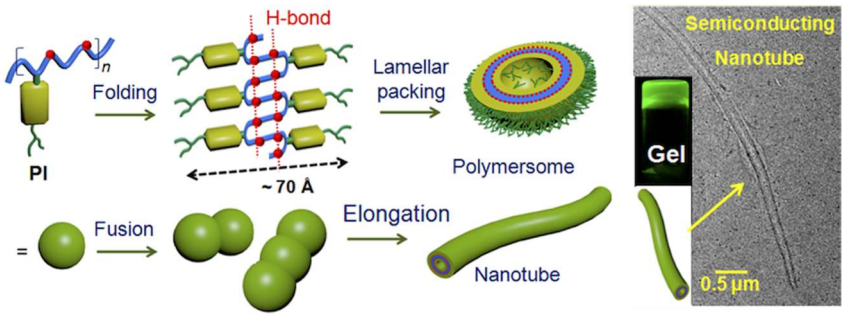

Figure 1. Schematic illustration of proposed self-assembly model of **P1**.
Reproduced with permission from Ref. 9. Copyright 2015 American Chemical Society.

absorption intensity varying linearly with concentration indicating "intrachain" NDI–NDI stacking. Therefore, folding of single polymer chains was supported. Corroborating these experimental observations, it was proposed (**Figure 1**) that **P1** spontaneously adopted a folded conformation in MCH by intrachain H-bonding among the urethane groups, leading to stacking of the pendant NDI units.

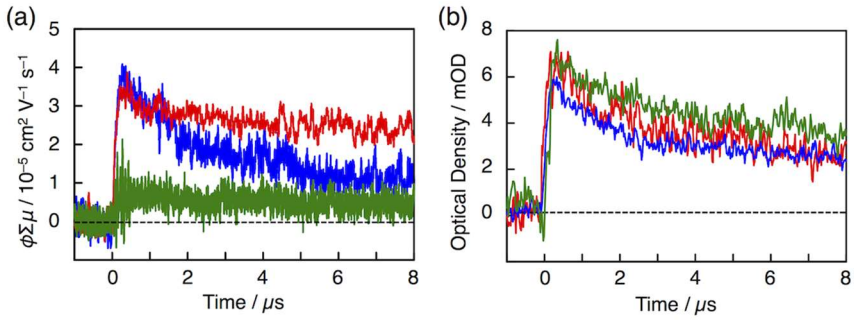

Figure 2. (a) Conductivity transients and (b) kinetic traces at 490 nm of transient absorption spectra for **P1** films dropcast from MCH gel (red), MCH solution (blue), and $CHCl_3$/MeOH solution (green) upon photoexcitation at 355 nm with photon density of 9.1×10^{15} photons cm^{-2} pulse^{-1}.

Noncontact evaluation of charge transporting property of polyurethane carrying NDI pendants.

The electron-transporting property of the well-defined supramolecular architectures of **P1** was studied by FP-TRMC. As noted earlier, FP-TRMC technique applies electric field of microwave that probes the local-scale charge carrier motions and thus enables the device-less evaluation of charge carrier transport. Upon photoexcitation by 355 nm laser pulses, a dried-gel film of **P1** on a quartz plate, prepared by drop-casting of MCH gel, showed a prompt rise followed by a slow decay in the conductivity transient (**Figure 2**), indicating that π-stacked NDIs in folded **P1** indeed provide charge transport pathways. In fact, a drop-cast film of **P1** from $CHCl_3$/MeOH solution, consisting of unfolded state of **P1**, displayed much smaller conductivity. The observed maximum $\phi\Sigma\mu$ values (3.5×10^{-5} cm^2 V^{-1} s^{-1} and ~0.7×10^{-5} cm^2 V^{-1} s^{-1} for gel in MCH and solution in $CHCl_3$/MCH,

respectively) indicated five times larger conductivity for **P1** in folded state compared to unfolded form. A dropcast film from freshly prepared MCH solution, including vesicle-shaped assembly, also showed a transient conductivity whose maximum value was quite similar to MCH gel state. In TAS, all the three films exhibited a characteristic absorption band at around 490 nm indicative of NDI radical anion species, where their kinetic profiles were similar to those of transient conductivity. Thus, electron transporting property was confirmed. After comparing the absorption coefficient of $NDI^{\bullet-}$ at 490 nm with the observed maximum TAS intensity, we evaluated the φ_{max} values as 1.5×10^{-2} and 1.8×10^{-2} for the dropcast films from MCH gel and $CHCl_3$/MeOH solution, respectively. These φ_{max} values are similar to that of reported organic crystals and thus indicate similar carrier generation mechanism. Finally, the electron mobility (μ_e) was calculated by combining the above ϕ_{max} and $(\phi\Sigma\mu)_{max}$ values. The calculated electron mobility values were 2×10^{-3} cm^2 V^{-1} s^{-1} and 4×10^{-4} cm^2 V^{-1} s^{-1} for the dropcast films from MCH gel and $CHCl_3$/MeOH solution, respectively, indicating strong impact of folded structure on charge carrier mobility. Of further interest, although the films from MCH gel and freshly prepared MCH solution showed the similar electron mobility, the former allowed much longer half- lifetime of charge carriers ($\tau_{1/2}$) than that from the latter ($\tau_{1/2}$ of ca. 40 and 5 μs, respectively). Taking into account this observation along with the fact that TRMC/TAS measurements were carried out under air, it is conceivable that confinement of NDI arrays within the folded polymer wall in nanotubularly assembled **P1** reduced the quenching probability by oxygen in one hand and provided long-range electron transporting pathways on the other hand, leading to the observed remarkable prolongation of negative charge carrier's lifetime.

Development of supramolecular polymers of porphyrin chromophores with amide functionalities.

ZnP (**Figure 3**) is a porphyrin derivative that undergoes living supramolecular polymerization[10,22,23] to afford nanofibers (**NF**) with *H*-aggregation of porphyrin chromophores or nanoparticles (**NP**) with *J*-aggregation. The presence of hexyloxy chains leads to the further integration of **NP**s into nanosheets (**NS**). These nanostructures are formed with the combination of π-π stacking of porphyrin cores, *H*-bondings of amide units, and van der Waals interaction of hexyloxy chains. **NP**s were prepared by the heat-cool procedure of **ZnP** in MCH. Then, aging of that solution resulted in the formation of **NS**s. On the other hand, sonication of **NP**s to prepare the seeds and addition of those into the initial solution gave **NF**s. The kinetic pathways of this system are summarized as a schematic illustration in **Figure 3b**. The morphologies of each nanostructure were clearly visualized by atomic-force microscopy (**Figure 3c–e**) and living polymerization nature was also confirmed. Due to the different π-π stacking geometry, the absorption spectra of

the three states are different from each other.

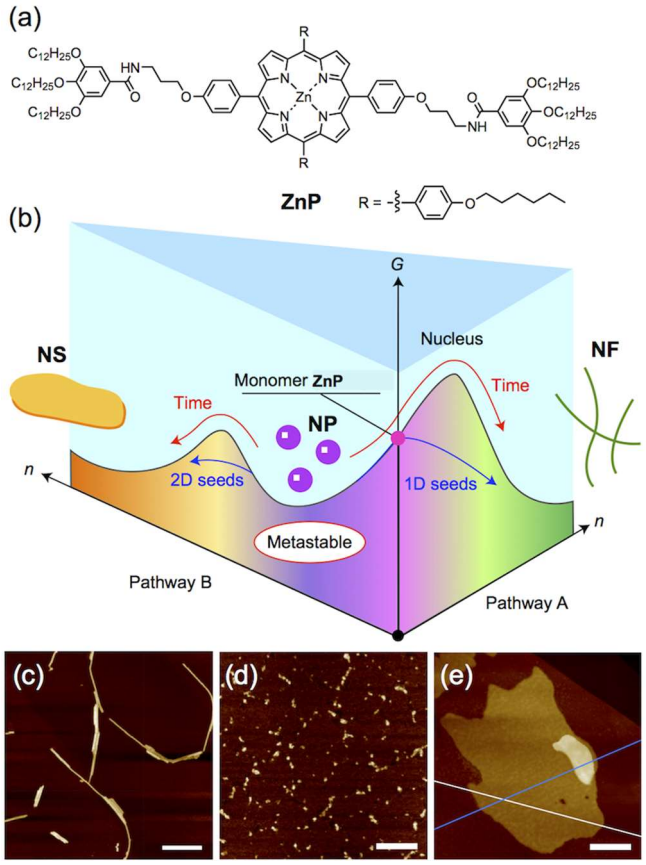

Figure 3. (a) Molecular structure of **ZnP**. (b) Differentiation of a metastable supramolecular assembly. Energy landscape of **ZnP** deduced from the mechanistic studies. AFM images of (c) **NF**, (d) **NP**, and (e) **NS**. Reproduced with permission from Ref. 10. Copyright 2017 Macmillan Publishers Ltd.

Noncontact evaluation of charge transporting property for supramolecular polymers of porphyrin chromophores.

The different π-π stacking behaviors of **ZnP** supramolecular polymer system motivated us to investigate the nanostructure-dependence on charge carrier transporting property. FP-TRMC measurements of dropcast samples revealed that **NF** showed the largest maximum transient conductivity $(\phi\Sigma\mu)_{max}$ of 2.6×10^{-5} cm^2 V^{-1} s^{-1}, while other two forms provided ca. four times smaller values (**Figure 4a**, **Table 1**). TAS measurements at the identical excitation condition of FP-TRMC disclosed the sign of generation of porphyrin radical cations, where kinetic traces of FP-TRMC and TAS are correlated each other (**Figure 4b–d**). These observation indicated that holes are dominantly transported along *H*/*J*- stacked-porphyrin cores under photoexcitation in ambient condition. By using the absorption coefficient of Zn porphyrin$^{\bullet+}$ at 600–650 nm with the observed maximum TAS intensity, we evaluated the ϕ_{max} values as 3×10^{-2}, $6 \times$

10^{-2}, and 6×10^{-2} for the dropcast samples of **NF**, **NP**, and **NS**, respectively (**Table 1**). Thus, the hole mobility was calculated as 9×10^{-4}, 1×10^{-4}, and 1×10^{-4}, respectively, by combining the above ϕ_{max} and $(\phi\Sigma\mu)_{max}$ values. The obtained values suggest that strong *H*-stacking of porphyrin cores in **NF**s is favorable for hole transport, while porphyrins in both **NP**s and **NS**s adopt *J*-aggregation and thus resulted in similar performance in local-scale hole transports.

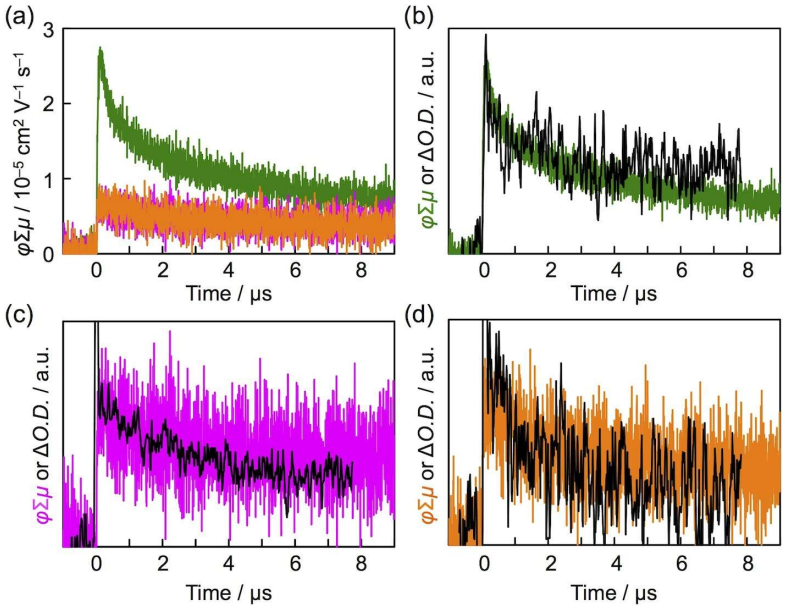

Figure 4. (a) Conductivity transients observed for **NF** (green), **NP** (magenta), and **NS** (orange) upon photoexcitation at 355 nm with photon density of 9.1×10^{15} photons cm^{-2} $pulse^{-1}$. (b) Normalized conductivity transients (green) and transient absorption at 620 nm (black) for **NF**. (c) Normalized conductivity transients (magenta) and transient absorption at 615 nm (black) for **NP**. (d) Normalized conductivity transients (orange) and transient absorption at 640 nm (black) for **NS**.

Table 1. Summary of $(\phi\Sigma\mu)_{max}$ and ϕ_{max} values evaluated by FP-TRMC and TAS measurements, together with calculated μ_{hole} values.

Entry	$(\phi\Sigma\mu)_{max}$ / cm^2 V^{-1} s^-	φ_{max} / –	μ_{hole} / cm^2 V^{-1} s^{-1}
NF	2.6×10^{-5}	3×10^{-2}	9×10^{-4}
NP	6.4×10^{-6}	6×10^{-2}	1×10^{-4}
NS	7.0×10^{-6}	6×10^{-2}	1×10^{-4}

Conclusion

Combination of FP-TRMC and TAS measurements revealed the strong impact of folded/unfolded structural difference of NDI-appended foldamer **P1** on the intrinsic electron mobility and carrier lifetime of the materials. Tuning of the structure of the appended π-conjugated cores would be a subject worthy of investigations for further

developing the supramolecular electronics.[24,25] Moreover, inspired by the *H*-bonding - directed assembly, an amide-appended porphyrin system with supramolecular living polymerization capability was studied. Depending on the nanostructures—nanofiber, nanoparticle, and nanosheet—the porphyrin chromophores adopt different stacking configurations. The contactless FP-TRMC/TAS method unveiled the different hole mobility depending on *H*/*J*- stacking self-assembly modes. Control of competitive intermolecular interactions including π-π stacking, *H*-bonding, and van der Waals would tailor the supramolecular materials with desired charge carrier transporting natures.

Acknowledgement

This research was supported by International Polyurethane Technology Foundation. S.S and S.G. acknowledge DST and JSPS for the grants of Bilateral Joint Research Projects (DST/INT/JSPS/P-218/2016). S.S. and M.T. acknowledge JSPS for Grant-in-Aid for Scientific Research on Innovative Areas "π-System figuration: control of electron and structural dynamism for innovative functions" (Numbers 26102009, 26102011, and 15K21721). T.S. acknowledges JSPS for Grant-in-Aid for Young Scientists (B) (Number 26810049) and (A) (Number 17H04880). K.S. acknowledges JSPS for Grant-in-Aid for Scientific Research on Innovative Areas "Dynamical ordering of biomolecular systems for creation of integrated functions" (Number 16H00787) and financial support from the Sekisui Chemical Grant Program.

References

(1) K. A. Houtona, A. J. Wilson, *Polym. Int.* **2015**, *64*, 165–173.

(2) M. Ding, J. Li, H. Tan, Q. Fu, *Soft Matter* **2012**, *8*, 5414–5428.

(3) A. Das, S. Ghosh, *Chem. Commun.* **2016**, *52*, 6860–6872.

(4) D. J. Hill, M. J. Mio, R. B. Prince, T. S. Hughes, J. S. Moore, *Chem. Rev.* **2001**, *101*, 3893−4011.

(5) G. Guichard, I. Huc, *Chem. Commun.*, **2011**, *47*, 5933–5941

(6) D.-W. Zhang, X. Zhao, J.-L. Hou, Z.-T. Li, *Chem. Rev.* **2012**, *112*, 5271−5316.

(7) S. Seki, A. Saeki, T. Sakurai, D. Sakamaki, *Phys. Chem. Chem. Phys.* **2014**, *16*, 11093–11113.

(8) A. Saeki, Y. Koizumi, T. Aida, S. Seki, *Acc. Chem. Res.* **2012**, *45*, 1193–1202.

(9) T. Mondal, T. Sakurai, S. Yoneda, S. Seki, S. Ghosh, *Macromolecules* **2015**, *48*, 879−888.

(10) T. Fukui, S. Kawai, S. Fujinuma, Y. Matsushita, T. Yasuda, T. Sakurai, S. Seki, M. Takeuchi, K. Sugiyasu, *Nature Chem.* **2017**, *9*, 493–497.

(11) W. E. Spear, *Proc. Phys. Soc.* **1957**, *B70*, 669–675.
(12) A. Tsumura, H. Koezuka, T. Ando, *Appl. Phys. Lett.* **1986**, *49*, 1210–1212.
(13) N. F. Mott, R. W. Gurney, *Electronic Processes in Ionic Crystals*, Oxford, London, **1940**.
(14) K. S. Cole, R. H. Cole, *J. Chem. Phys.* **1941**, *9*, 341–351.
(15) A. Acharya, S. Seki, A. Saeki, Y. Koizumi, S. Tagawa, *Chem. Phys. Lett.* **2005**, *404*, 356–360.
(16) A. Saeki, S. Seki, T. Sunagawa, K. Ushida, S. Tagawa, *Philos. Mag.* **2006**, *86*, 1261–1276.
(17) A. Saeki, S. Seki, Y. Koizumi, S. Tagawa, *J. Photochem. Photobio. A* **2007**, *186*, 158–165.
(18) J. C. Slater, *Rev. Mod. Phys.* **1946**, *18*, 441–512.
(19) (a) S. Tomonaga, *J. Phys. Soc. Japan.* **1947**, *2*, 158–171. (b) S. Tomonaga, *J. Phys. Soc. Japan.* **1948**, *3*, 93–105.
(20) P. P. Infelta, M. P. de Haas, J. M. Warman, *Radiat. Phys. Chem.* **1977**, *10*, 353–365.
(21) R. J. O. M. Hoofman, M. P. de Haas, L. D. A. Siebbeles, J. M. Warman, *Nature* **1998**, *392*, 54–56.
(22) S. Ogi, K. Sugiyasu, S. Manna, S. Samitsu, M. Takeuchi, M. *Nature Chem*. **2014**, *6*, 188–195.
(23) S. Ogi, T. Fukui, M. L. Jue, M. Takeuchi, K. Sugiyasu, *Angew. Chem. Int. Ed.* **2014**, *53*, 14363–14367.
(24) T. Mondal, K. Dan, J. Deb, S. S. Jana, S. Ghosh, *Langmuir* **2013**, *29*, 6746–6753.
(25) T. Mondal, S. Ghosh, *Polym. Chem.* **2016**, *7*, 6735–6743.